IEEE TRANSACTIONS ON

GEOSCIENCE AND REMOTE SENSING

JULY 1985 VOLUME GE-23 NUMBER 4 (ISSN 0196-2892)

A PUBLICATION OF THE IEEE GEOSCIENCE AND REMOTE SENSING SOCIETY

SPECIAL ISSUE ON SATELLITE GEODYNAMICS

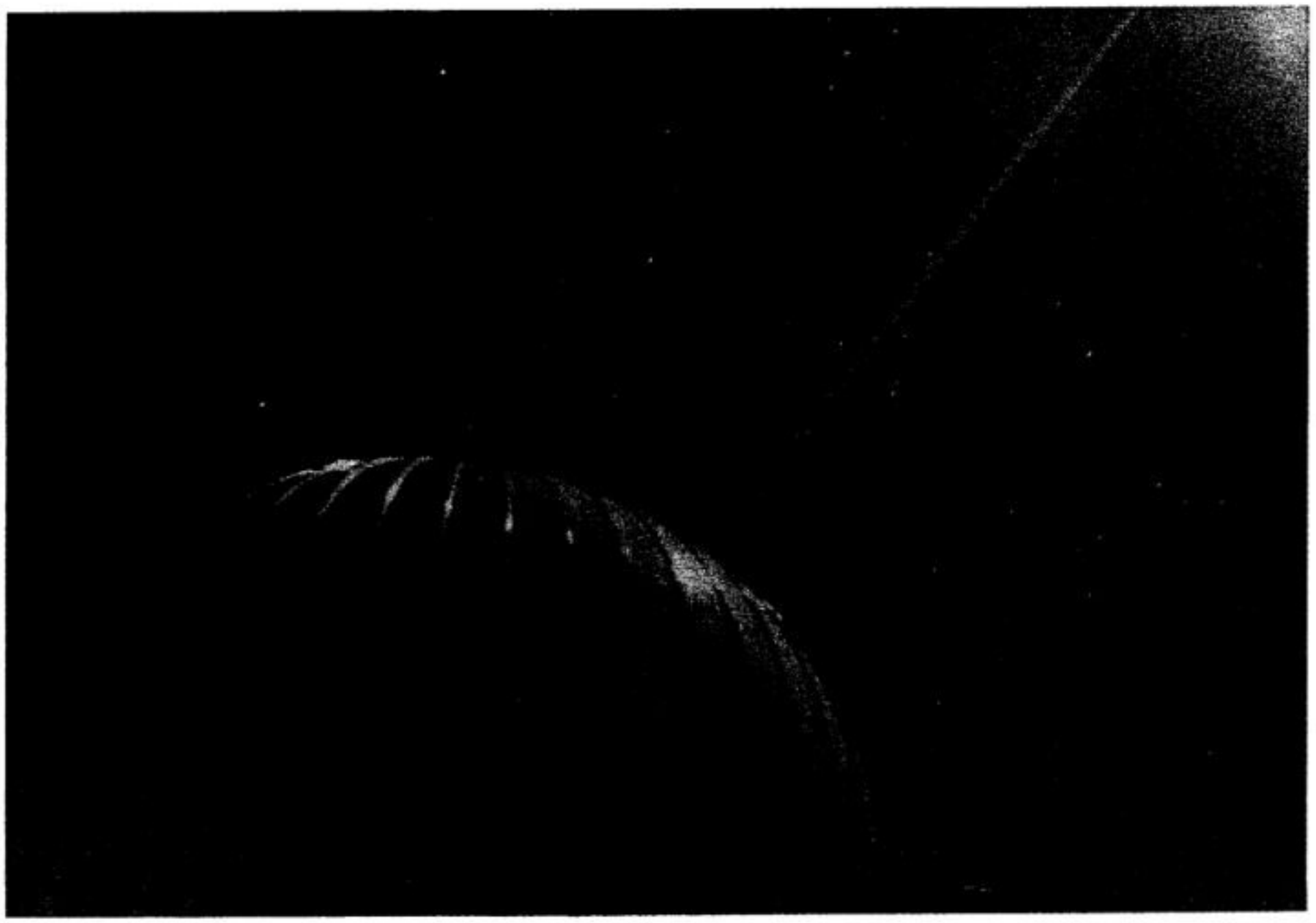

Laser Ranging from Haleakala Observatory, Maui, Hawaii.

Satellite Laser Ranging: Current Status and Future Prospects

JOHN J. DEGNAN

Abstract—**This paper is intended to be a nonmathematical tutorial on the subject of satellite laser ranging (SLR) with an emphasis on the characteristics and capabilities of present and future field-hardware and operational methods. Following a brief introduction to the basic concept of SLR and the many science applications of both satellite and lunar laser ranging, we discuss the developmental history of each of the major components which make up the ranging machine, i.e., the laser transmitter, photomultiplier, discriminator, and time interval unit. At the same time, we attempt to identify the sources of range error in each of the devices and present, whenever possible, experimental data which quantifies the magnitude of these errors. We also describe some of the subtleties associated with the operation of these devices in the field. Following the discussions on hardware and system calibration techniques, we briefly describe some error sources external to the basic ranging machine, but highly relevant to SLR, which are introduced by the target, atmospheric channel, ground surveys, epoch timekeeping, geopotential models, and numerical propagation errors. We summarize the description of modern day hardware with samples of actual satellite data, obtained as early as 1981, which show orbital fits with a 1.5 cm single shot rms and normal point rms of less than 3 mm with only 1–6 percent data editing. We conclude the paper with a discussion of ongoing research to develop systems potentially capable of millimeter absolute accuracies over satellite distances. These advanced systems make use of dual wavelength ultrashort pulse laser transmitters and streak camera-based range receivers.**

I. Introduction

THE FIRST laser range measurements to an artificial satellite equipped with optical retroreflectors took place at NASA's Goddard Space Flight Center (GSFC) in 1964 [1]. A Q-switched ruby laser was used to measure the distance to the Beacon Explorer B satellite with a precision of a few meters. Since that time, approximately 14 retroreflector-equipped satellites have been placed in Earth orbit. Today, a global network of both fixed and mobile satellite laser ranging (SLR) systems routinely ranges to a subset of these satellites. The Laser Geodynamics Satellite (LAGEOS), launched in 1976, is the primary target, however, since it was designed specifically to support a variety of science applications. LAGEOS is a 60-cm-diameter sphere whose surface is studded with a total of 426 cube-corner reflectors. The heavy (441 kg) satellite is in a stable well-defined orbit at an altitude of 5900 km, and therefore functions as a reference point in inertial space. By ranging to it, sets of ground-based laser systems can recover their relative geometry or their position with respect to the Earth's center of mass or, alternatively, their position with respect to an inertial reference. The few-centimeter accuracy of modern SLR systems, therefore, permits the development of greatly improved geopotential models, better estimates of the Earth's internal mass distribution, and global geodesy with accuracies of 2–5 cm over continental distances. A time record of these measurements yields data on tectonic plate motion, polar (Chandler) wobble, and variations in the Earth's rotation rate or length of day. A recent review of the scientific uses of SLR data can be found in a comprehensive NASA Headquarters report [2].

In addition to artificial satellites, a total of five planar retroreflector arrays have been landed on the moon. Three of the lunar arrays were placed there by the astronauts of Apollo 11, 14, and 15 while two French-built arrays were carried by two unmanned Soviet spacecraft, Lunakhods 1 and 2. Lunar laser ranging (LLR) data provides detailed information on Earth-lunar dynamics including the motion of the center of mass (lunar ephemeris), rotations about the center of mass (librations), the internal mass distribution (moments of inertia), and lunar tides. In addition, LLR experiments have provided highly accurate measurements of the gravitational constant–Earth mass product (i.e., GM) and served as tests of competing theories of general relativity. The scientific accomplishments of lunar laser ranging have been reviewed by Mulholland [3] and Alley [4] while a description of one of the earliest and most successful LLR stations at the McDonald Observatory has been provided by Silverberg [5].

Fig. 1 is a simplified block diagram of a typical ground-based SLR system. A portion of the outgoing laser pulse is detected by the range receiver which, in turn, starts a time-of-flight measurement. The remainder of the pulse propagates through the atmosphere and is reflected by the satellite retroreflectors back through the atmosphere into the receiving telescope. The telescope collects and focuses the returning radiation onto the photocathode of a high-gain high-speed photomultiplier and the resulting return signal stops the time-interval counter. A digital word, representing the round-trip time of flight of the pulse, is stored by the system computer along with other information to be described later.

Satellite laser ranging stations are now located globally in over twenty countries and on every continent except Antarctica [6]. Many stations are located at multiuser telescope facilities and hence are fixed. Since 1969, NASA has developed a total of eight trailer-based mobile laser

Manuscript received February 8, 1985; revised March 1, 1985.

The author is with the Instrument Electro-Optics Branch, Code 723, NASA Goddard Space Flight Center, Greenbelt, MD 20771.

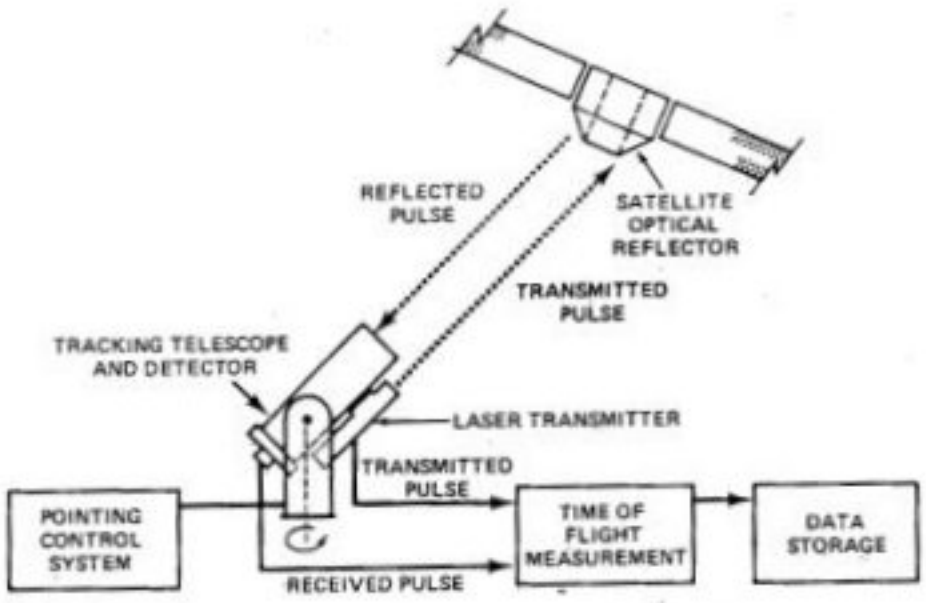

Fig. 1. Satellite laser ranging system concept.

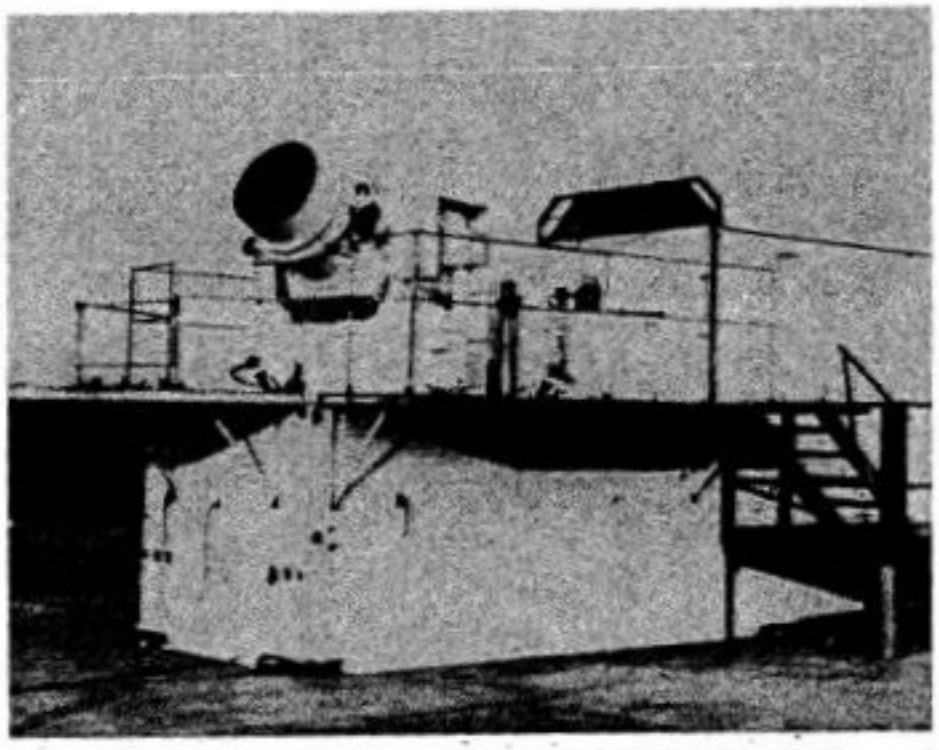

Fig. 2. NASA/GSFC mobile laser (MOBLAS) tracking station.

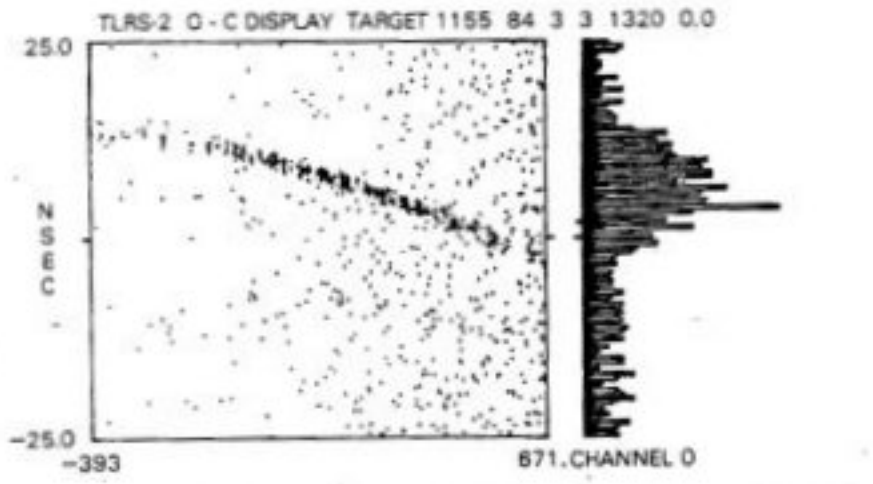

Fig. 3. Single photoelectron TLRS-2 raw range data near dawn at Cabo San Lucas, Mexico, 1984.

Fig. 4. TLRS-3 undergoing field tests at GSFC.

(MOBLAS) ranging stations, shown in Fig. 2, capable of occupying a variety of sites in support of tectonic plate studies. A similar European version is becoming operational this year. More recently, a new breed of highly compact transportable laser ranging systems (TLRS) were developed in response to a need of the geophysics community to obtain SLR data at remote sites and to be rapidly relocated in support of tectonic plate studies. The first of these systems, TLRS-1, was developed by the University of Texas and is contained within a small camper van. It has been described in detail by Silverberg and Byrd [7]. The second operational system, TLRS-2, was developed at GSFC. The latter system is housed in a small number of standard shipping containers which can be carried in aircraft cargo bays and reassembled quickly at remote sites, such as Easter Island on the important Nazca plate.

The compact size of the TLRS systems was achieved at the expense of greatly reduced operational signal levels (two orders of magnitude lower) resulting from a considerably smaller telescope aperture (10 in versus 30 in) and lower laser output energies (5 mJ versus 100 mJ) when compared to the larger trailer-based MOBLAS systems. On the average, a single-photoelectron satellite return is received only about once per twenty firings of the laser. Thus the return is distinguishable from background noise only through its association with other closely spaced points from previous firings. This is illustrated in Fig. 3 which shows a 20-min segment of raw LAGEOS range data obtained by TLRS-2 at Cabo San Lucas, Mexico, in 1984. The horizontal scale is in seconds relative to the point of closest approach (PCA) of the satellite pass. The vertical scale gives the observed minus calculated (OMC) range in nanoseconds. The satellite returns are clearly visible as a dark line against a background of random noise counts. This figure is particularly interesting since the data was taken near dawn and there is a clear increase in background noise as we move from left to right on the horizontal time scale. The single-photoelectron TLRS systems employ special multistop time interval counters which permit up to 7 separate time-interval measurements, or stop signals, for each start pulse. This increases the data yield by allowing the detection of several background-noise counts without disabling the time-interval counter prior to the actual satellite return. During 1985, two smaller higher performance versions of TLRS-2 will be deployed. The first of these, TLRS-3, is shown at its GSFC test site in Fig. 4.

Because of the large Earth to lunar distances and the

fact that return signal strengths vary inversely with the fourth power of range, LLR stations are also characterized by small detection probabilities in spite of the fact that they use the highest power transmitters and the largest scientific telescope apertures. Instead of time interval counters, these systems employ highly accurate event timers which record and "time tag" individual "single-photoelectron events" without necessarily labeling them as "start," "stop," or "noise" pulses. This permits the LLR station to increase its data yield by operating at high laser repetition rates (e.g., 10 pps) without regard to the relatively long 2.5-s lunar time of flight.

In the remainder of this article, we will focus on the developmental history and current status of the hardware used in modern satellite laser ranging systems. We will attempt to identify and explain, in nonmathematical terms, the dominant error sources in modern centimeter-accuracy instrumentation and to describe current efforts to develop millimeter-accuracy sytems.

II. Ranging Components and Error Sources

A. Laser Transmitter

Early satellite ranging systems used Q-switched ruby lasers. These lasers were capable of generating very high output energies, on the order of several joules, in a pulse several tens of nanoseconds wide. Since the ruby laser is very inefficient and requires large power sources to drive the flashlamps, later systems employed more compact and efficient Nd:YAG lasers which also had shorter Q-switched pulsewidths on the order of 10 ns or less. Shorter pulse-widths reduce the random ranging error contribution of the contribution of the transmitter which varies as $\tau_p/\sqrt{N}$ where τ_p is the FWHW laser pulsewidth and N is the number of received photoelectrons.

It soon became apparent that Q-switched lasers exhibited variable biases which were undesirable in a precision satellite laser ranging system. These biases arise from the multimode nature of Q-switched lasers. In such lasers, individual radiation modes, both "spatial" and "temporal," build up at their own rates and are coupled to the external world by a partially reflecting mirror which forms one end of a two-mirror laser cavity. Furthermore, different spatial modes have different far-field radiation patterns. This results in a range bias which is dependent on the angular position of the target in the transmitter far-field pattern. This effect has become known in the laser-ranging community as "wavefront-distortion" error. In addition, the magnitude of the bias has been observed to vary slowly with time [8] suggesting that the radiated-mode structure is a function of laser temperature.

An early approach to reducing the bias errors in Q-switched lasers was to pass the laser pulse through an external "pulse slicer" consisting of an electrooptic Pockels cell situated between two crossed polarizers. Only the central 4–5 ns of the typically 20-ns pulse would be transmitted to the satellite. Although this technique was relatively easy to implement in the field, it was rather inefficient since it rejected a sizable fraction of the laser energy.

A short-lived interim solution to this problem was the development of the pulse transmission mode (PTM) or "cavity-dumped" Nd:YAG laser. This is also a multimode device, but the radiation modes are trapped inside the laser cavity until they are simultaneously "dumped" by an internal electrooptic switch [8]. Thus since all modes leave the transmitter at the same time, the angularly dependent range bias is greatly reduced. With subnanosecond switching times, cavity-dumped lasers have pulsewidths on the order of 2–3 ns corresponding to the time it takes light to make one round trip in the laser cavity.

The transmitter laser in the most modern field systems consists of a mode-locked Nd:YAG laser oscillator followed by one or more Nd:YAG laser amplifiers. Since mode-locked Nd:YAG lasers operate in a single spatial mode (i.e., the fundamental TEM_{00} mode having a Gaussian spatial profile), they do not exhibit the aforementioned "wavefront-distortion" errors. Individual longitudinal ("temporal") modes are "locked" together, by either a passive dye or active acoustooptic or electrooptic modulator internal to the laser resonator, to create pulsewidths as short as 30 ps. A passive nonlinear crystal, such as Potassium Dideuterium Phosphate (KD*P), converts the fundamental infrared radiation of the Nd:YAG laser material at 1.06 μm to the 0.53-μm green frequency-doubled wavelength, with 40–50 percent efficiency, in order to take advantage of more sensitive photodectectors available in the visible-wavelength region.

A typical SLR transmitter, such as that used in NASA's mobile laser (MOBLAS) tracking network, produces a single optical pusle with a pulsewidth between 150 and 200 ps and a single pulse energy of about 100 mJ at the frequency-doubled green wavelength. The pulse repetition rate is typically 5 pulses/s. With these energies and repetition rates, data sets of more than 10 000 range measurements (up to 80-percent data return) have been obtained in a clear atmosphere for a single high-elevation LAGEOS pass lasting approximately 45 min.

Table I lists the ranging performance of various laser types tested at GSFC [9]. The list includes three conventional stable-resonator (denoted by S) Q-switched lasers as well as one unstable resonator device (denoted by U), three PTM Q-switched ("cavity dumped") lasers, and three mode-locked transmitters. Two standard tests were performed for each laser transmitter: a "repeatability test" and a "far-field range map" [9].

In the repeatability test, a groundbased target is centered in the laser-beam and range measurements are made for approximately 45 min corresponding to the time it takes to complete a high-elevation LAGEOS satellite pass. For each set of 100 range measurements, a mean and standard deviation is calculated and plotted versus elapsed time.

The range-map test is designed to quantify the range biases resulting from the high-order mode effects ("wavefront distortion") discussed previously as a function of target position in the transmitter far-field pattern. In per-

TABLE I
LASERS TESTED BY GSFC

TYPE	MANUFACTURER	PULSEWIDTH (FWHM)	REPEATABILITY	RANGEMAP
Q-SWITCHED (S)	GENERAL PHOTONICS (MOBLAS)	7 NSEC	POOR	POOR
Q-SWITCHED (S)	MODIFIED GENERAL PHOTONICS	4 NSEC	FAIR (1PPS) POOR (5PPS)	FAIR (1PPS) POOR (5PPS)
Q-SWITCHED (S)	WESTINGHOUSE (MILITARY)	8 NSEC	POOR	POOR
Q-SWITCHED (U)	QUANTA-RAY	5 NSEC	VERY GOOD	POOR
PTM Q-SWITCHED	INTERNATIONAL LASER SYSTEMS (LL102)	4 NSEC	EXCELLENT	FAIR
PTM Q-SWITCHED	GENERAL PHOTONICS	3.6 NSEC	EXCELLENT	FAIR
PTM Q-SWITCHED	NASA-MODIFIED GP	1.5 NSEC	VERY GOOD	VERY GOOD
ACTIVE MODE-LOCK	INTERNATIONAL LASER SYSTEMS	225 PSEC	EXCELLENT	EXCELLENT
PASSIVE MODE-LOCK	QUANTEL INTERNATIONAL YG40 AND YG402	60 PSEC, 150 PSEC	EXCELLENT	EXCELLENT

CRITERIA FOR RANGING PERFORMANCE RATINGS

RATING	PEAK-TO-PEAK VARIATION IN 100 POINT MEAN
POOR	EXCEEDS 20 CM PEAK-TO-PEAK
FAIR	BETWEEN 10 AND 20 CM PEAK-TO-PEAK
GOOD	BETWEEN 6 AND 10 CM PEAK-TO-PEAK
VERY GOOD	BETWEEN 2 AND 6 CM PEAK-TO-PEAK
EXCELLENT	LESS THAN 2 CM PEAK-TO-PEAK

forming the test, the direction of the transmitter beam is varied so that the target lies at different points within the transmitter far-field pattern. At each position, two 100-point data sets are taken and a mean range and standard deviation is calculated for each set. The mean range with the target at beam center is then subtracted from the means at the other target positions to determine the dependence of range bias on far-field angle.

As can be seen from Table I, the performance of mode-locked transmitters is far superior to that of other laser types. Bias effects introduced by mode-locked transmitters, either active or passive, are typically at the subcentimeter level [9].

B. Photomultiplier

Almost all field SLR systems currently use conventional dynode-chain photomultiplier tubes (PMT's). In the latter devices, the incoming light pulse impinges on a photocathode with a quantum efficiency on the order of 10–15 percent. The resulting short burst of photoelectrons is then accelerated through a potential difference to an adjacent dynode where electron multiplication, or gain, takes place. The electrons continue to multiply as they propagete from dynode to dynode until they finally arrive at the anode. Gains of 10^6 are typical for PMT's used in SLR systems.

The time it takes the electrons to propagate from the photocathode to the anode via the intervening dynodes is referred to as the "transit time." This represents a fixed temporal delay, or bias, introduced into the time-of-flight measurement. It varies with the PMT bias voltage and can be on the order of tens of nanoseconds (meters). This delay is just one of many optical, electronic, or cable delays occurring in a typical ranging system. Fortunately, the overall "system delay," which corresponds to the sum of delays introduced by individual components or propagation lengths, can be accounted for, or possibly eliminated, via calibration procedures or common channel receiver techniques to be discussed later.

Variations in the transit time are referred to as "transit time jitter" and represent a random uncertainty superimposed onto the measurement. Many of the best dynode-chain PMT's, such as the "electrostatic" and "static crossed-field" tubes introduced by Varian Inc., attempted to minimize this "jitter" by providing a well-defined path for the electrons to follow through the use of controlling electrostatic or magnetic fields. Unfortunately, this path is only well defined if the starting point, the focal spot on the photocathode, is also fixed. Pointing errors in a real tracking system, however, will cause the satellite image to move about within the photocathode. This can cause variations, as large as 1 ns (15 cm), in the systematic PMT transit time as the satellite image moves from center of the photocathode to the edge [10].

Recently, the microchannel-plate photomultiplier (MCP/PMT), has been introduced. Photoelectrons generated by the photocathode are accelerated over a short gap of about 0.6 mm ("proximity focusing") by a bias voltage and impinge on the face of a microchannel plate. The latter is made up of a closely packed array of narrow cylindrical channels with diameters on the order of 10 μm. Once inside a channel, the photoelectron ricochets repeatedly off the cylindrical inner wall generating more electrons in the process. Typically, three such plates must be stacked together to achieve gains in excess of 10^6.

Since the MCP tubes are characterized by much-shorter and better-defined electron-path lengths, they exhibit much shorter transit times and smaller jitters than conventional dynode-chain PMT's. For example, the ITT F4128 MCP PMT has a transit time delay of only a few nanoseconds. More importantly, the path of the electron is tightly con-

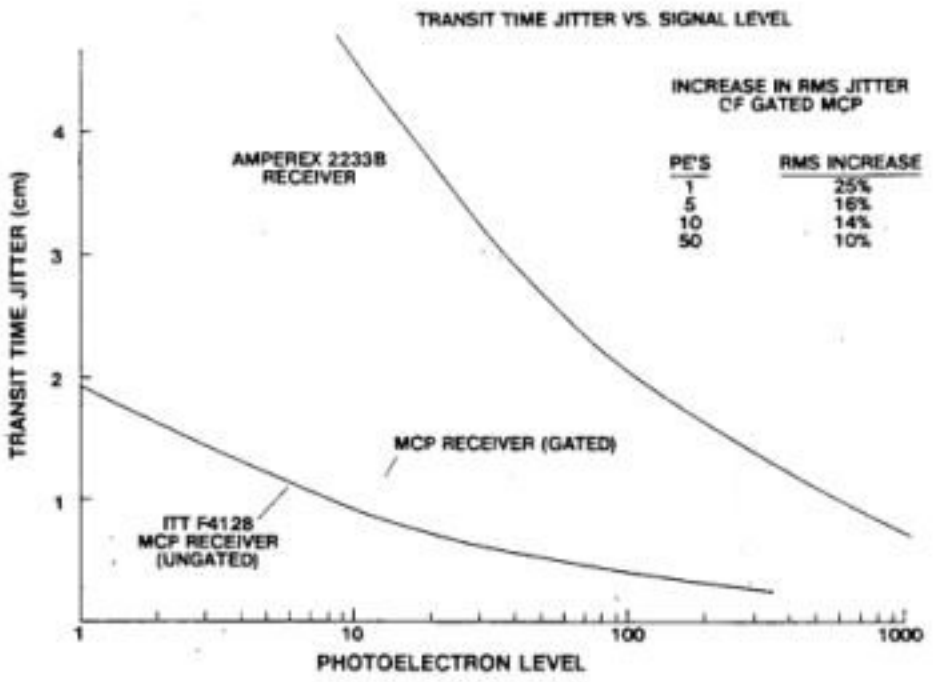

Fig. 5. A comparison of transit time jitter as a function of signal level for the Amperex 2233B dynode chain PMT and the ITT F4128 microchannel-plate PMT (gated and ungated).

trolled by the high bias voltage appled over the narrow acceleration gap and through confinement by the narrow microchannel. This results in an extremely small transit time jitter. Furthermore, since the transit time varies only weakly with the starting position of the photoelectron, the MCP exhibits a greatly reduced sensitivity to image-position effects and the resulting biases appear to be less than 3 mm [10].

During daylight operations, it is sometimes desirable to "gate" the PMT. Gating of the tube is accomplished by applying the acceleration, or bias, voltage only during a time period when the returning laser pulse is expected. This inhibits the propagation of photoelectrons from the photocathode to the first dynode or microchannel and prevents background optical noise from saturating the electron amplification stages. The ideal "gate" voltage pulse is short in duration (typically a few microseconds or less), has a fast rise and fall time, is very flat in the temporal region where the pulse is expected, and has a highly repeatable amplitude. If the latter requirements are not met, the gate will severely degrade the timing performance of the PMT.

Fig. 5 compares the performances of the ITT F4128 MCP PMT with that of an Amperex 2233B dynode-chain PMT currently used in the NASA MOBLAS network [11]. The one sigma transit time jitter for an ungated MCP tube is about 2 cm for single-photoelectron inputs compared to 10 cm in the 2233B. For input signal levels of eight photoelectrons or more, the jitter is subcentimeter in the MCP/PMT. The jitter increases between 10 and 25 percent, depending on signal level, for one particular gating configuration developed at Goddard. The MCP/PMT also has an impulse response of 450 ps compared to 4 ns for the 2233B. The faster impulse response improves the performance of the timing electronics to be discussed next.

The ITT F4128 contains two internal MCP amplifier stages and has an electron gain of 2×10^5. In our upgrade recommendations to the network, the F4128 was chosen over the higher gain F4129 model, with three stages and a gain of 3×10^6, because of the former's greater tolerance for the higher background radiation levels associated with daylight tracking of satellites. The lesser gain can be compensated for by the inclusion of a 1-Ghz bandwidth amplifier available from ENI. One gigahertz is an adequate bandwith since the 450-ps PMT impulse response is usually degraded to about 1 ns by propagation through long receiver cables in typical field systems.

There is some evidence to suggest that the transit time can also be influenced by the amplitude of the input signal or by a higher background of noise photons [12]. Experiments with the Amperex 2233B PMT suggest that the tube transit time decreases with an increase in the photon background rate. Changes in the 2233B transit time on the order of a centimeter have been observed for background count rates of 4×10^6 at typical PMT operating voltages and the transit time decreased rapidly for count rates in excess of 10^7. Similar studies have not yet been performed on microchannel PMT's.

To summarize, factors which can influence the performance of a photomultiplier in a laser ranging system are: 1) impulse response, 2) transit time jitter, 3) the position of the image on the photocathode, 4) the amplitude of the input signal, and 5) background radiation. The microchannel-plate photomultiplier offers several important advantages over conventional dynode-chain PMT's.

C. Discriminator

The output from the photomultiplier/amplifier, which is typically a quasi-Gaussian waveform with a randomly varying amplitude, is input to a constant fraction discriminator (CFD). The discriminator defines the point on the signal waveform on which the timing will be based and generates a rectangular NIM logic pulse having a few nanosecond width which, in turn, starts or stops the time interval unit. Although varying signal amplitudes in other discriminator types (such as fixed threshold, rise-time compensated, and hybrids) will cause time biases on the order of half the input pulse width, the bias is highly repeatable and can be taken out with a software correction if the signal amplitude is measured and recorded with each range measurement. The CFD, on the other hand, includes hardwired circuitry which attempts to compensate for a varying signal level. A plot of time bias versus signal amplitude is a measure of the degree to which the aforementioned compensation circuitry has been successfully implemented and is often referred to as the "time-walk characteristic" of the discriminator.

Fig. 6 displays the time-walk characteristics for the ORTEC 934 CFD, currently used in the MOBLAS network, and a relatively new CFD, the Tennelec TC453 [11]. Both discriminators were adjusted for minimum time walk with a 1-ns full-width half-maximum-input pulsewidth. To generate the curve, start and stop pulses separated by a fixed interval are generated elecronically. The amplitude of the stop pulse is varied by means of an attenuator. Each point on the time-walk characteristic represents the mean of 100 time-interval measurements made at a particular

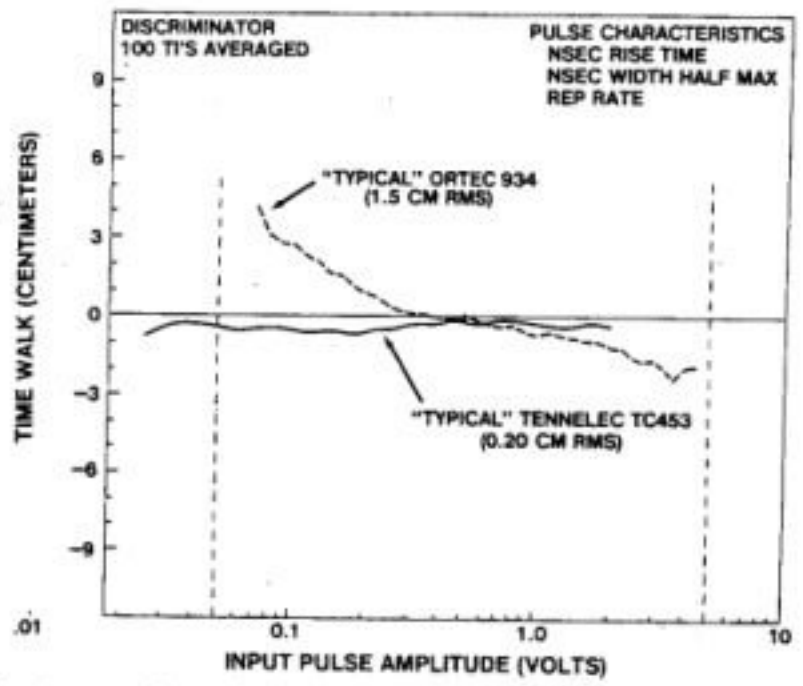

Fig. 6. A comparison of discriminator time walk as a function of signal level for the ORTEC 934 and the Tennelec TC453.

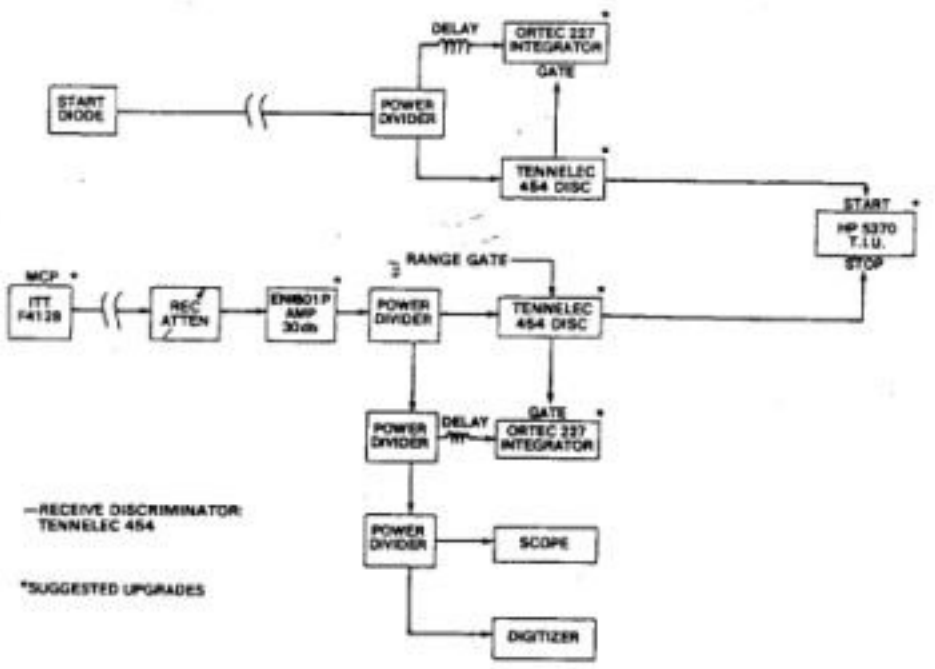

Fig. 7. An upgraded dual-channel range receiver proposed for MOBLAS.

stop-signal amplitude. Thus the time-walk characteristic is a measure of the expected signal-amplitude-dependent bias imposed by the discriminator on the range measurement. The standard deviation about the mean value (not shown) is then clearly the random uncertainty associated with the amplitude-dependent bias correction.

The vertical dashed lines in Fig. 6 represent the specified dynamic range of the ORTEC unit. As one can easily see from the figure, the TC453 has a much flatter time-walk characteristic. The rms deviation from the nominal zero point is about 0.2 cm over the full dynamic range compared to 1.5 cm for the older ORTEC device.

Tennelec also offers a four-channel gatable version of their basic CFD, the TC454. The discriminator is gated by means of a low-voltage rectangular logic pulse. This permits the temporal interval, during which an incoming "stop" signal will be accepted, to be narrowed to as little as 10 ns (1.5 m) although other considerations, such as uncertainty in target range, will usually dictate larger gate widths on the order of 100 ns or more.

Discriminator gating reduces the false-alarm rate produced by background radiation through *temporal* filtering of the incoming counts. Narrow-band optical filters in front of the PMT further discriminate against noise through *spectral* filtering of the incoming light. The discriminator also permits rejection of background noise via the *amplitude* of the incoming pulse. Amplitude filtering is accomplished by adjusting the discriminator threshold so that it will trigger only when a prescribed minimum voltage level (e.g., 1–3 photoelectrons) is input to it. In practice, the discriminator threshold is usually raised until the frequency of noise counts received from the sky background is at an acceptable level. Setting the threshold too high will result in a lower probability of detection for the range return and a reduced data yield. Furthermore, since returns that are just above threshold are in the high time-walk region of the discriminator characteristic (see Fig. 6), it is usually desirable for the mean signal level to lie well above the threshold setting. Thus the final threshold setting will represent a compromise between these competing effects. Fortunately, at night the background count is usually so low that one can set a threshold just above the single photoelectron level and even occasionally dispense with the optical filter to increase the optical throughput of the receiver. Needless to say, daylight tracking is a completely different situation. In systems designed to operate at the single-photoelectron level, such as the TLRS systems, one clearly loses the ability to "amplitude" filter the data.

D. Time Interval Unit

The purpose of the time interval unit (TIU) is to measure the time of flight of the optical pulse. Fig. 7 shows a dual-channel range-receiver configuration which has been recommended to the NASA MOBLAS network for the next round of performance upgrades. It utilizes many of the state-of-the-art commercial components previously discussed. In a dual-channel range receiver, the outgoing pulse is detected by a photodiode and input to the start discriminator while the incoming pulse is detected by the higher gain PMT and input to the stop discriminator. A logic pulse from the start discriminator starts the time interval measurement and a corresponding pulse from the stop discriminator stops it. Almost all field SLR systems use single-stop time interval units. Presently, the Hewlett-Packard HP 5370A time interval counter, which has a 20-ps time resolution and 100-ps accuracy, is recommended for field operations.

A noise pulse which enters the receiver prior to the satellite return and exceeds the stop discriminator threshold will disable a single-stop TIU and prevent it from timing the actual range return. For multiple-photoelectron systems operating at night, the impact on data yield is negligible. During daylight operation, however, the added background may force the imposition of more severe spectral or amplitude filtering of the incoming radiation with all of the attendant negative influences (e,g., reduced optical throughput, increased discriminator time walk and jitter, etc.) on the quantity and quality of the range data. In these instances, a multistop TIU, capable of detecting

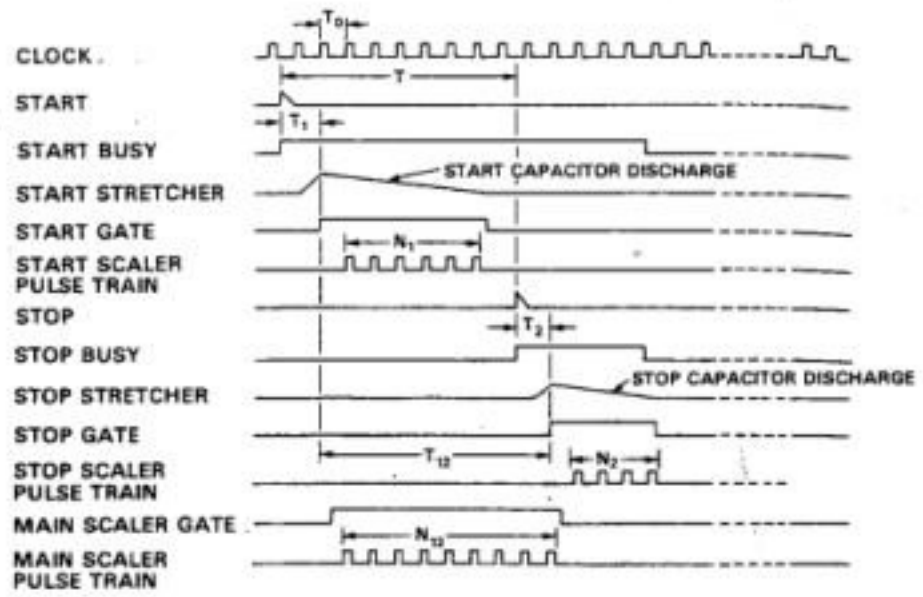

Fig. 8. Timing diagram for a 9.76-ps resolution time interval unit built for NASA by Lawrence Berkeley Laboratories.

and timing one or more stop pulses relative to the start pulse, permits receiver threshold and gain settings to be nearer their optimum values during daylight operation. Unfortunately, most commercial multistop time interval units have inferior time resolutions on the order of 1-ns. Developmental multistop TIU's with 78-ps resolution, however, exist at the Lawrence Berkeley Laboratories (LBL) [13] and units with 10-ps timing resolution are well within the state of the art [14].

Not all TIU's work in precisely the same manner, but they do have a number of common components and features which permits us to discuss the dominant error sources in a fairly general way. We will use as our model a single-stop TIU built for NASA by LBL which has a 9.76-ps resolution and a maximum range of 340 ms [14]. The corresponding timing diagram in Fig. 8 will be the focus of our discussion.

The heart of the TIU is a very stable clock, or master oscillator, which produces a train of pulses at a "fixed" rate, (typically 50 MHz) and ultimately determines the absolute accuracy and stability of the TIU. The measured time interval T is defined as the temporal separation between the leading edges of a pair of logic pulses applied externally to the start and stop inputs of the digitizer by the corresponding discriminators. The time measurement is split into three parts, i.e., $T = T_1 + T_{12} - T_2$ as detailed in Fig. 8. T_1 is the interval between the leading edge of the start pulse and the second following master clock pulse. T_2 is similarly defined as the interval between the leading edge of the stop pulse and the second following clock pulse. T_{12} is the interval between the two aforementioned clock pulses and is measured by counting the number of intervening clock pulses in a binary scaler, i.e., $N_{12} = T_{12}/T_0$ where T_0 is the master clock period.

To accurately measure the smaller components T_1 and T_2, the latter are "stretched" in two identical time-to-time converters called "interpolators." The stretching constant k is an integer and selected to be $k = T_0/T_e$ where $T_0 = 20$ ns is the master clock period and T_e is the desired timing resolution. A value $k = 2048$ in the LBL unit implies a timing resolution $T_e = 9.766$ ps.. Competing TIU's generally differ in their approach to the interpolators. In the LBL unit, the arrival of the start pulse causes a capacitor to be charged at constant current over the small time interval T_1. The capacitor is then discharged by a constant current k times smaller than the charging current. A comparator monitors the triangular current waveform across the capacitor and generates a square gate pulse k times longer than the original charging interval. This gate passes a burst of N_1 clock pulses which are in turn counted by a binary start scaler. The number of pulses counted by the binary start scaler is given by $N_1 = kT_1/T_0$. Similarly, an identical interpolator on the stop side counts N_2 clock pulses given by $N_2 = kT_2/T_0$. Thus the measured time interval is given by

$$T = T_0(N_1/k + N_{12} - N_2/k).$$

Instead of capacitors, the HP5370A TIU uses a second clock, which is slightly offset in frequency from the master oscillator, and coincidence timing to stretch the T_1 and T_2 time intervals. The start pulse initiates the second clock and the start scalar counts pulses from the master clock until coincident pulses from the two clocks are detected to yield the value T_1. The time T_2 is measured similarly. A smaller frequency offset implies a longer period between coincidence pulses and hence a larger stretching constant.

The error introduced by the TIU is now seen to be

$$\Delta T = T\Delta f_0/f_0 + T_e(\Delta N_1 - \Delta N_2)$$

where $\Delta f_0/f_0$ is the stability of the external master oscillator and ΔN_1 and ΔN_2 are the interpolator conversion errors.

Considering the first term in the error equation, we see that a fixed offset Δf_0 in the nominal clock frequency will result in a range-dependent bias error. On the other hand, a varying Δf_0 representing clock phase noise will introduce a random error in the measured range. For subcentimeter-accuracy ranging to the LAGEOS satellite ($T > 5 \times 10^{-2}$ s), a clock accuracy of one part in 10^{10} is required. To achieve the same precisions over lunar distances ($T > 2.5$ s), one would need an accuracy of a few parts in 10^{12}.

To minimize the interpolator conversion errors ΔN_1 and ΔN_2 the start and stop interpolator components are carefully selected and matched to take advantage of the fact that the two interpolator time intervals are subtracted from each other. Propagation delays of the start and stop input signals through the interpolators are made as short and as equal as possible to eliminate time offset errors and minimize temperature effects. The measured thermal stability of the LBL-designed unit is about 3.0 ps/°C. High bandwidth components are used to improve the phase synchronization of the interpolators with the master oscillator, and fast risetime discriminators aid in the precise definition of the beginning and end of the elapsed time interval. Since the start and stop inputs are typically dc coupled, any noise superimposed on the baseline of the start and/or stop signals can result in a timing error due

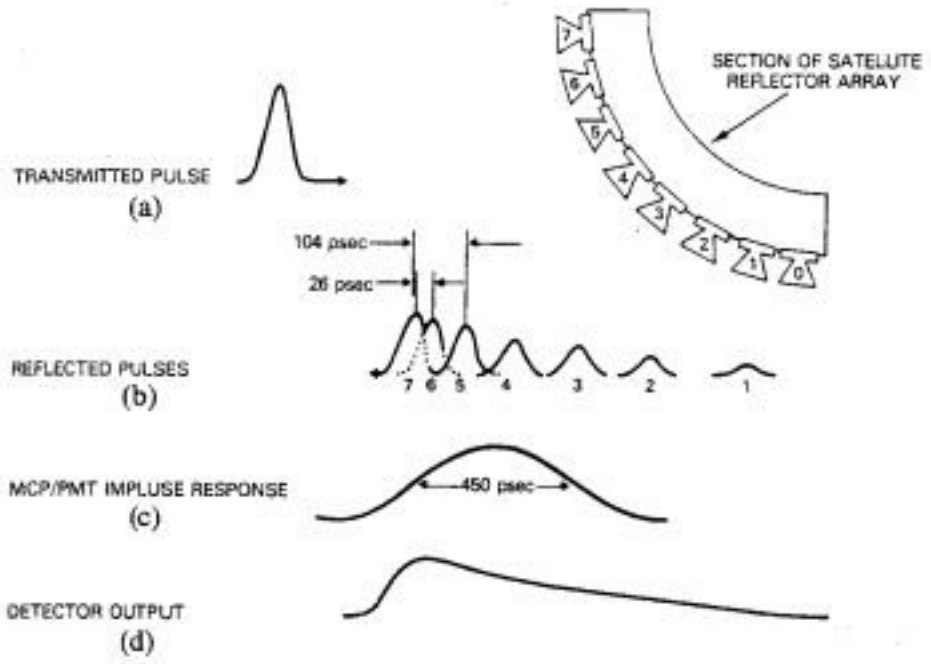

Fig. 9. LAGEOS induced pulse spreading.

to a time shift in discriminator firing. Major contributors to timing jitter include component noise, power supply ripple, and clock-frequency lock-in noise [14].

E. Target Effects

The mechanical design of the LAGEOS satellite places the front face of the solid-cube-corner reflectors (CCR's) at a distance of 298.1 mm from the center of the satellite. When one takes into account the size and index of refraction of an individual CCR, it can be shown that reflection effectively takes place on a sphere 258 mm from the satellite center of gravity (CG) and this systematic bias must be added to the measured range.

The impulse response of the satellite is not expected to be exactly spherically symmetric, however, due to the finite number of CCR's. The response of an individual cube to incoming radiation drops off to zero as the angle of incidence relative to the normal of the solid cube face increases to a maximum of about 25°. Thus approximately 10–15 adjacent cubes contribute to the return signal seen at the receiver. For a sufficiently short laser pulse and a sufficiently fast receiver response, it is conceivable that individual cubes, or rows of cubes, could be detected—at least at some satellite orientations such as in Fig. 9. The integrating effect produced by a few-hundred-picosecond PMT response, however, leads to an asymmetric spreading to the pulse return, as illustrated in Fig. 9, which will cause the CG correction to be a function of both satellite orientation and pulsewidth.

Actual measurements of the CG correction at GSFC prior to launch, using leading-edge half-maximum timing, yielded an average value of 251 mm with a standard deviation of 1.3 mm and a peak-to-peak variation of less than ±3 mm over all orientations of the LAGEOS satellite [15]. For centroid detection, the correction was 249 mm with a standard deviation of 1.7 mm. The measured CG correction varied by 8.1 mm as the laser pulsewidth was varied from 62 ps (253.8 mm) to 1000 ps (245.7 mm). Thus the proper CG correction varies, at the few-millimeter level, as a function of satellite orientation, laser pulsewidth, receiver strategy (leading edge versus peak detection), and receiver impulse response.

Finally, the 200-ps pulsewidths currently used in the most advanced SLR systems are long enough such that the individual cube returns overlap in time and their corresponding electric fields interfere coherently at the receiver in a totally unpredictable fashion. This "coherent fading effect" is sensitive to geometric changes on the order of a wavelength and, hence, there is no correlation on time scales corresponding to the laser fire period of 0.2 s. No direct measurements of this effect were possible during prelaunch testing, but theoretical calculations suggest that "coherent fading" will introduce a random timing error with a standard deviation of 77 ps (1.15 cm) [15].

Only LAGEOS and Starlette are spherical in shape. All of the other retroreflector-equipped satellites utilize one or more planar arrays, and the induced pulse spreading is a strong function of the angle of incidence of the impinging radiation relative to the array normal. This clearly causes a significant time-varying bias error in the range measurement, which can only be removed if the satellite orientation relative to the ground station is known reasonably well at all times during the pass.

F. Atmospheric Refraction Errors

As the laser pulse traverses the atmosphere, it sees a varying refractive index resulting primarily from spatial variations in the local pressure with only a weak dependence on local temperature and humidity. The varying refractive index influences the propagating pulse in two ways. The most important effect from a laser ranging standpoint is a varying group velocity, i.e., the pulse speeds up as it travels from the ground station to low-pressure regions at the higher altitudes. The second effect is a consequence of Snell's law of refraction which predicts a bending of the light ray as it moves through atmospheric layers having different refractive indices thereby resulting in a curved ray path. Thus in order to convert time of flight to an absolute geometric range, we must be able to account for the cumulative effect of the refractive-index variation on the pulse transit time.

The total bias introduced by the atmosphere is substantial, amounting to about 2.5 m at zenith and growing to 13 m at elevation angles of 10°. Atmospheric models, which assume a spherical-shell model of the atmosphere and which use surface measurements of pressure, temperature, and relative humidity at the site as inputs, are currently used to eliminate the vast majority of the induced bias error. The residual error sources following application of the model clearly include 1)inadequacies of the model (e.g., ignoring the variation of atmospheric parameters with latitude and longitude and imperfect knowledge of the variation with altitude) and 2) errors in the measurement of the various surface meteorological parameters used by the model. It is currently believed, based on a limited amount of ray-tracing data, that the residual bias error from these sources is between 0.5 and 1.5 cm.

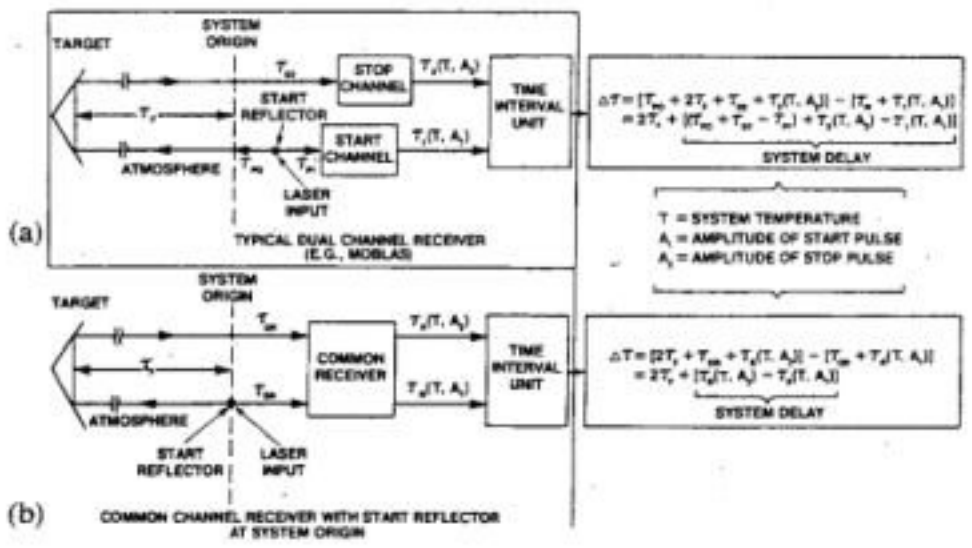

Fig. 10. Origins and elimination of system delay (instrument range bias): (a) conventional dual-channel range receiver; (b) "zero delay" common channel receiver.

The current state of knowledge in this area is reviewed in a companion paper in this journal. [16].

Atmospheric turbulence has a correlation time scale on the order of 1 ms and, therefore, imposes an additional random error on the range measurement at current system fire rates. For typical atmospheric conditions and elevation angles, the rms deviations are a few millimeters or less but can grow to a few centimeters under conditions of strong turbulence at low elevation angles (10°) [16]. Range data, however, is never taken under conditions of strong turbulence or at elevation angles below 20°.

G. System Delay Calibration

The goal of a laser ranging system is to measure the geometric distance between a fixed reference point within the system (the system "origin") and the external target. A common choice for system origin is the point at which the telescope azimuth and elevation rotation axes intersect. The system actually measures the round-trip time of flight of the laser pulse between the two points plus a "system delay." Fig. 10(a) illustrates the origins of system delay in a conventional dual-channel laser ranging system. A portion of the outgoing laser pulse is deflected at time $\tau = 0$ by a beam splitter into the start photodiode at time τ_{p1} while the remainder travels to the target and back to the stop photomultiplier in a time $\tau_{p0} + 2\tau_f + \tau_{02}$. In traveling through the photodetectors, amplifiers, discriminators, and connecting cables to the time interval unit, the start and stop pulses experience additional electronic delays given by τ_1 (T, A_1) and τ_2 (T, A_2), respectively. The latter are functions of the ambient temperature T and the amplitudes of the start and stop signals A_1 and A_2 as we have seen from our discussion of discriminator time walk. Other operational variables, such as PMT operating voltages, discriminator threshold, electronic attenuator settings, etc., also influence the system delay but, barring operator error, these are kept constant in a given satellite pass.

The method currently employed to estimate system delay is to make repeated range measurements (typically a few thousand) to a calibration target a "known" distance away from the system origin immediately before and after each satellite pass ("pre- and postcalibration"). This "known" time of flight ($2\tau_f$ in Fig. 10) is then subtracted from the measured time of flight $\Delta\tau$ to yield the overall system delay. The received signal levels are varied over the dynamic range expected from the satellite by means of an optical attenuator. Range means are then computed for signals falling within each amplitude range. During reduction of the satellite data, the latter information can be used to correct for the amplitude dependence of the system delay.

When Q-switched lasers were used as transmitters, it was not uncommon to see large variations (centimeters) between the pre-and postcalibration means. The pre- and postcalibration runs in the most modern field systems which employ mode-locked transmitters, however, generally agree to within a few millimeters (see Table I). Nevertheless, even subcentimeter-precision laser ranging systems can have few-centimeter absolute errors if the reference standard, i.e., the "known" distance to the calibration target, is in error by this amount. Currently, these standards are obtained by making collocated continuous-wave laser-geodimeter measurements at the ranging site. Obvious error sources include systematic calibration and random resolution errors associated with the geodimeter reference and variable but systematic atmospheric effects (which can be substantial over several-kilometer paths at extremely low elevation angles) [17]. Furthermore, it is usually not possible to position the geodimeter at or very near the system origin since the latter is internal to the ranging system or tracking telescope. Hence, there is an additional error associated with estimating the position of the geodimeter relative to the ranging-system origin. Based on repeated site surveys over a period of several years, past experience would suggest that the repeatability in the geodimeter measurements is no better than about 2 cm. As system precisions improved to the centimeter and even subcentimeter levels, the accuracy of the system delay calibration took on increased importance and became a subject for serious investigation.

The basic problem is to define an optical link such that the time of flight $2\tau_f$ over the calibration range can be truly known with the desired accuracy. To make maximum use of the capabilities of modern hardware, one should strive for an absolute accuracy on the order of a few millimeters. If possible, the calibration should be applied to each and every range measurement so that long-term drifts and instabilities in the ranging machine can be taken out of the data.

An obvious improvement to the conventional technique is to move the calibration target sufficiently close to the system reference plane so that the intervening distance can be measured with a measuring tape or rod. This approach would clearly eliminate all of the uncertainties associated with system calibration mentioned previously but is not always feasible for a given optical design in an existing field system. Furthermore, multistop or redundant TIU's would be required to self-calibrate on every out-

going laser pulse. Silverberg [18] has described one such field implementation of a self-calibration scheme in the single-photoelectron TLRS-1 system. Fiberoptic calibration paths have also been suggested. To be successful, the fibers should be short enough so that uncertainties in the effective index of refraction (group velocity) due to material inhomogeneities, dispersion, fiber bending, temperature effects, etc., are negligible. Furthermore, common timing electronics must be used to the maximum extent possible.

Fig. 10(b) illustrates a somewhat different approach to system delay calibration currently being investigated at Goddard. In this approach, both the start and stop pulses utilize a common photodetector and timing channel so that the electronic system delay cancels except for calibratable signal-amplitude effects. Thus any time-dependent variations in the electronic system delay caused by ambient temperature variations, etc., cancel out in this "common-channel-receiver" approach (which can be implemented with the HP 5370A TIU described previously). If, in addition, the optical propagation paths are made collinear and a reflector is placed at the system origin to deflect the start pulse into the PMT, the start and stop optical delays will also cancel and the system will have an expected bias of zero, i.e., no system delay.

The ease with which a zero-delay system can be implemented depends heavily on the design of the transmitter and receiver optical trains. It requires the use of transmit/receive switches (e.g., active electrooptic or rotating mirror switches or passive polarization-dependent switches) to control the start- and stop-signal amplitudes on the photodetector and is easiest to implement on refractive collecting telescopes. Zagwodzki *et al.* [19], however, have described one implementation of the "zero-delay" scheme, shown in Fig. 11, which is currently being evaluated at a new experimental satellite laser ranging facility located at the Goddard Optical Research Facility. The transmitted laser beam is expanded to fill the 1.2-m diameter primary of a coude-focus cassegrain telescope. A retroreflector, located in a plane normal to the azimuth axis and containing the elevation axis and system origin, reflects a small fraction of the outgoing laser pulse into the common start/stop channel of the range receiver to start the time-interval measurement. The start signal into the PMT is attenuated by reflection off an AR-coated area on a rotating-mirror transmit/receive (T/R) switch and by several neutral density filters rotating with the mirror. Several nanoseconds earlier, the same components aid in reducing the level of scatter when the output laser pulse is transmitted through the same AR coating. By the time the stop pulse returns many milliseconds later from the satellite, a highly reflecting surface is in place to maximize the throughput to the PMT.

Dual-channel field systems such as MOBLAS can also be readily modified to permit common channel ranging. In these systems, the laser beam is transmitted via a small refractive telescope adjacent to the receiver telescope. A fraction of the outgoing laser pulse can be deflected via

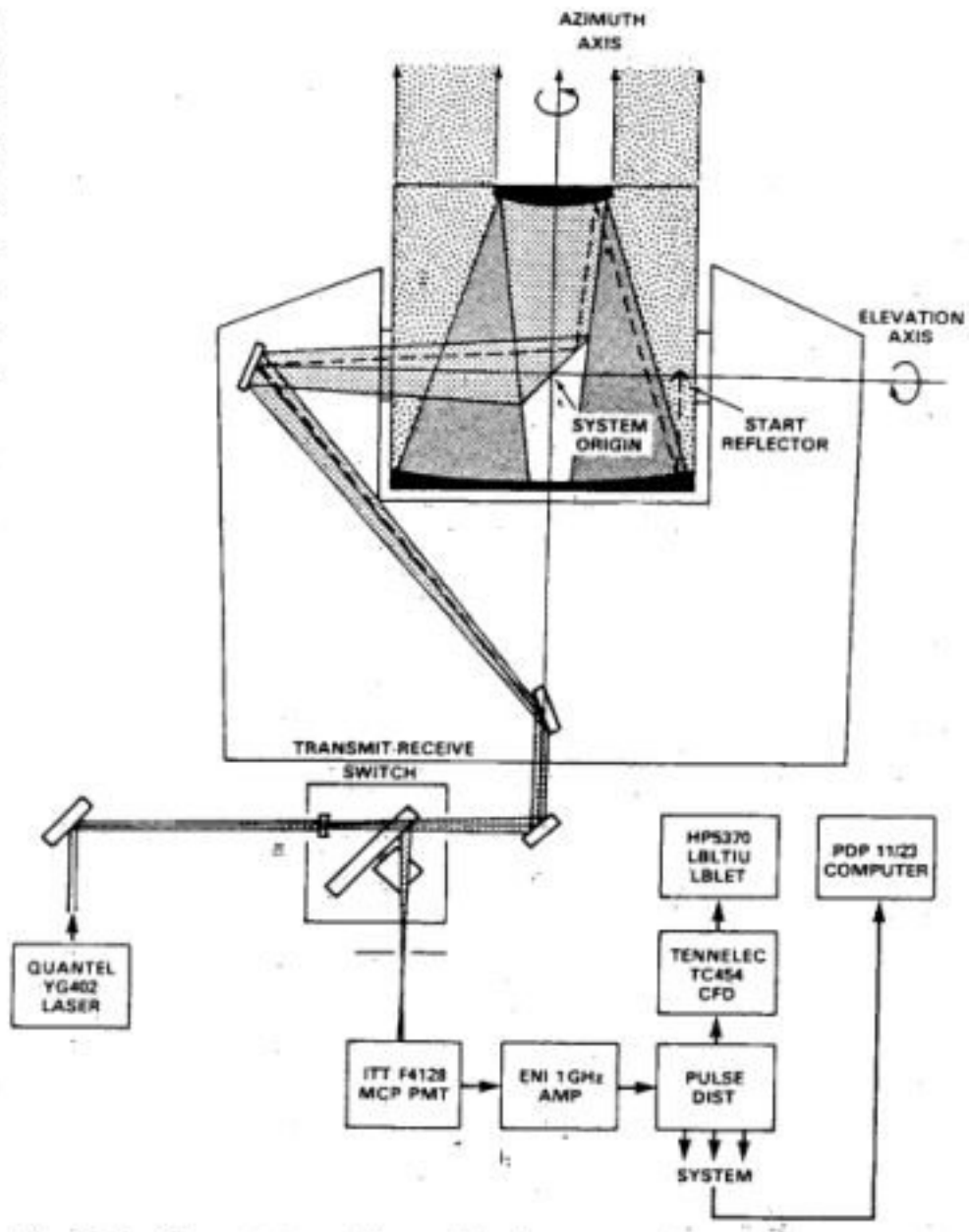

Fig. 11. Implementation of "zero delay" common-channel range receiver in experimental satellite laser ranging system (ESLRS) at Goddard's 1.2-m telescope facility.

mirrors into the receiving telescope aperture and attenuated, if necessary, to provide a start pulse to the range receiver. In this manner, the receiver electronic delays cancel (except for signal amplitude effects) and, since the start and stop pulses follow a common optical path from the receiver telescope aperture to the receiver PMT, most of the optical delay also cancels. The residual optical delay is sufficiently short that it can be measured very accurately with a steel tape or rod. In a MOBLAS system, for example, the residual delay would correspond to the relatively short optical-path length followed by the diverted transmitter start pulse as it propagated from the system reference plane, through the diverting mirrors, to the receiver telescope aperture.

H. Error Sources External to the Ranging Machine

Before a developmental SLR station is deployed into the field, it undergoes a "collocation test" in which two or more stations, located within about 60 m of each other, range simultaneously to a common satellite. When possible, one of the stations is a "standard" with a good performance record. The close proximity between stations simplifies the data analysis and assures a common refraction path through the atmosphere. The purpose of the test is to detect and identify the source of any system biases through reduction and comparison of the satellite range

data obtained by the two stations. Even after deployment, intercomparisons between the satellite range data taken at different stations can point out discrepancies at a particular station via the global model fit. Such intercomparisons will also be sensitive to errors which are external to the ranging machine and to the atmospheric channel. For the sake of completeness, we will discuss them briefly.

One example is a systematic error in epoch time often referred to as a "time-tag" error. This is the difference between "station time" as determined by the station clock and "universal time." Depending on the sign of the difference, the satellite will be either farther along or lagging behind in its orbit relative to its expected location based on "station time." This clearly has an impact not only on the agreement between observed and calculated range (about 4 mm/μs of epoch-time error) but also on the systems ability to acquire and track the satellite. Thus a time standard, such as LORAN-C, is required at each site to maintain epoch time to within 1 μs with respect to a master clock such as the one at the U.S. Naval Observatory in Washington, DC. At remote sites such as Easter Island, timekeeping is performed with about 50-ns accuracy by a rubidium clock referenced to a global positioning system (GPS) receiver [20]. The rubidium clock is stable enough to maintain time for short periods when the GPS satellites are not accessible. The GPS system can also provide initial estimates of station position in unsurveyed areas by interrogating 4 or more satellites in the GPS satellite constellation.

Errors in station location can also be detected in the data reduction process. This is the position of the system reference or origin relative to some fiducial marker or survey monument in an earth-based geodetic reference system.

Discrepancies between the observed and calculated range to a satellite can also be caused by deficiencies in the orbital model, inaccurate interrange-vector (IRV) (see Section III) data input to the model, or numerical propagation errors in long arc computations.

The various error sources inherent in a satellite laser ranging system are summarized in Table II.

TABLE II
ERROR SOURCES FOR SATELLITE LASER RANGING

ERROR SOURCE	TYPE ERROR	RECOMMENDED INSTRUMENTATION
TRANSMITTER		
1. MULTIMODE EFFECTS	SYSTEMATIC	• QUANTEL YG402DP MODELOCKED LASER 150 PSEC FWHM
2. PULSE SHAPE VARIATIONS	RANDOM	
RECEIVER		
1. OPTICAL SNR	RANDOM	• MULTIPLE PHOTOELECTRON CAPABILITY
2. PHOTODETECTOR		• MICROCHANNEL PLATE PMT (ITT F4128)
• RESPONSE TIME	SYSTEMATIC	
• TRANSMIT TIME JITTER	RANDOM	
• AMPLITUDE EFFECTS	SYSTEMATIC	
• IMAGE POSITION EFFECTS	SYSTEMATIC	
• BACKGROUND	SYSTEMATIC	
3. SUB-OPTIMAL FILTER/ AMPLIFICATION	SYSTEMATIC	• ENI 601P AMPLIFIER
4. DISCRIMINATORS		• TENNELEC TC 454 WITH SOFTWARE AMPLITUDE CORRECTION VIA ORTEC 227 INTEGRATOR
• AMPLITUDE DEPENDENT TIME WALK	SYSTEMATIC	
• SINGLE SHOT JITTER	RANDOM	
• PULSEWIDTH DEPENDENCE	RANDOM	
5. TIME INTERVAL UNIT		• HP 5370A
• CLOCK OFFSET	SYSTEMATIC	
• CLOCK PHASE NOISE	RANDOM	
• INTERPOLATOR LINEARITY AND TRACKING	SYSTEMATIC	
• INTERPOLATOR RESOLUTION	RANDOM	
6. EPOCH TIME	SYSTEMATIC	• GPS TIME TRANSFER RECEIVER
SYSTEM DELAY CALIBRATION		
1. SURVEY ACCURACY		• COMMON TRANSMIT/RECEIVER CHANNEL
• GEODIMETER RESOLUTION	RANDOM	• START REFLECTOR AT SYSTEM ORIGIN
• ATMOSPHERIC EFFECTS	SYSTEMATIC	• FREQUENT AMPLITUDE CALIBRATION
• GEODIMETER POSITION	SYSTEMATIC	
2. CALIBRATION DRIFT	SYSTEMATIC	
ATMOSPHERE		
1. METEROLOGICAL SENSOR	SYSTEMATIC	• FREQUENT MET SENSOR CALIBRATION
2. MODEL ERRORS	SYSTEMATIC	• TWO COLOR RANGING WITH STREAK CAMERA
3. TURBULENCE	RANDOM	
SATELLITE ERRORS		
1. CENTER OF GRAVITY CORRECTION	SYSTEMATIC	
2. COHERENT FADING	RANDOM	
3. ORBITAL MODEL DEFICIENCIES	SYSTEMATIC	• IMPROVED ORBITAL MODELS
OPERATOR ERRORS		
1. PHOTOMULTIPLIER/ AMPLIFIER SATURATION	SYSTEMATIC	• CONTROL SIGNAL LEVELS
2. INFREQUENT OR IMPROPER CALIBRATION/TEST PROCEDURES	SYSTEMATIC	• DIAGNOSTIC INSTRUMENTATION • REGULAR CALIBRATION SCHEDULE
OTHER ERRORS		
1. STATION LOCATION	SYSTEMATIC	

III. Acquisition and Tracking

In order to acquire and track the satellite, an IRV consisting of a position and velocity vector for the target satellite at a specific time t is provided to the tracking computer. The tracking computer integrates the orbital equations of motion using a fairly simple geopotential field model and performs a series of coordinate transformations to control the azimuth and elevation axes of the optical mount to arcsecond accuracies. Absolute pointing at the arcsecond level is not possible unless one takes into consideration the effects of mechanical fabrication and alignment tolerances and "sag" within the optical mount which produce pointing errors varying with azimuth and elevation angle. These errors are taken out by means of a star-calibration procedure. In this procedure, the telescope is commanded to point to as many as fifty stars. The angular bias errors in both axes are measured and recorded for each star position. The bias errors are fit, in a least squares fashion, to a two-dimensional polynomial in azimuth-elevation space. This, in turn, provides an interpolated software correction for any pointing angle contained within the solid angle defined by the star set. In pointing to the satellite, a software correction is also made for the effects of atmospheric refraction on the "apparent" angular position of the satellite, i.e., optical ray bending resulting from the variation of atmospheric refractive index with altitude. The model utilizes ground-based measurements of surface pressure, temperature, and relative humidity at the site. Furthermore, all field systems incorporate an operator-adjusted device for inserting a time bias into the pointing commands to correct for along track errors. Similarly, cross-track errors in pointing can be eliminated with the appropriate angular biases.

IV. LAGEOS Ranging Results with a Partially Upgraded Receiver

In the summer of 1981, a passively mode-locked Nd:YAG laser transmitter was installed in the MOBLAS 4 station at the Goddard Optical Research Facility, Green-

TABLE III
SATELLITE-PASS SUMMARY

DATE	RETURNS	POINTS REJECTED	SINGLE SHOT RMS SYS CAL	SINGLE SHOT RMS PASS	NORMAL PNT. RMS (50 AV)	PRE/POST	NOTES
BEC PASSES							
10/8/81	450	16.8%	2.7CM	2.7CM	.5CM	0.0CM	2233PMT
10/9/81	287	10.1%	1.3	2.67	.4	.4	MCPPMT
LAGEOS PASSES							
9/25/81	2420*	3.5%	5.6	3.7	.8	0.0	2233PMT
9/26/81	3717	3.0%	3.6	4.2	1.2	- 8.1*	2233PMT
9/29/81	3510	8.0%	5.5	2.5	1.0	-25.8*	2233PMT
10/9/81	86	17.0%	1.41	1.68	.05	1.97	MCPPMT
10/14/81	2594	6.7%	1.18	1.77	.27	0.0	MCPPMT
10/15/81	5286	4.7%	1.62	2.56	.83	.66	MCPPMT
10/17/81	1877	3.3%	1.15	1.51	.24	.39	MCPPMT
10/20/81	3083	2.6%	1.28	1.68	.30	.88	MCPPMT
10/20/81	2963	1.7%	2.3	2.2/2.0	.4	0.0	MCPPMT
10/21/81	315	24%	2.24	4.1	.79	- .63	MCPPMT
11/3/81	594	4.3%	1.4	2.1	.37	- .58	MCPPMT

*DUAL HISTOGRAM FROM TARGET POLE REFLECTION (SEE TEXT)

belt, MD. Satellite tracking tests were initially performed using the standard operational receiver which consisted of the Amperex 2233B PMT, the ORTEC 934 constant fraction discriminator, and the HP 5360 Time Interval Unit. After taking 3 LAGEOS and 1 BEC pass with the standard receiver, the 2233B PMT was replaced by a prototype of the ITT 4129 microchannel-plate PMT. The latter had only a 5 percent quantum efficiency compared to the 12–15 percent of current commercial devices. Because of the shorter pulsewidth out of the MCP/PMT, it was necessary to adjust the ORTEC 934 CFD for short-pulse operation by means of an external cable delay. The ranging performance of the standard and upgraded systems was evaluated using the software package LASPREP which fits the raw range data to a simple orbit (including geopotential terms up to J3) using the best least squares estimates of range and time bias, applies a three sigma filter to the data, and repeats the procedure until there is no further improvement in the rms of the orbital fit. The software also computes running normal points which are obtained by averaging 50 returns and then dropping the first data point in the subset and adding the subsequent data point to compute the next normal point.

Table III summarizes the results of the field experiments [11]. Using the Amperex 2233B PMT with the mode-locked laser resulted in single-shot rms precisions to LAGEOS between 2.5 and 4.2 cm, as determined by the LASPREP processor, for three separate passes in September 1981. The Rms precision of the normal points was between 0.8 and 1.2 cm. In these runs, anywhere from 3 to 8 percent of the raw data was edited out by the iterative processor. Interestingly, the satellite data was better than the ground pre- and postcalibration data. This apparent inconsistency was later traced to a support pole behind the calibration target which reflected spurious pulses into the receiver and resulted in a double-peaked range calibration histogram.

After painting the offending pole black and installing the microchannel-plate PMT, agreement between the pre- and postcalibrations was typically subcentimeter with one exception (1.97 cm) for the 9 LAGEOS passes. The single-shot rms for the system calibration runs fell between 1.1 and 2.3 cm. The single-shot rms for the LAGEOS data sets was only slightly higher than for the calibration data sets, i.e., typically between 1.5 and 2.5 cm for large data sets. Only 1–6 percent of the raw range data was edited by the processor in obtaining these results. Extensive laboratory tests have suggested that 1.5 cm is about the limit of precision achievable with the older HP 5360 TIU and that the latter was the limiting error source in the field receiver. Similar tests with the newer HP 5370A TIU typically yield a factor of 3 better precision, i.e., a single-shot precision of about 0.5 cm. Nevertheless, the satellite normal point rms was impressive, varying between 0.05 and 0.83 cm over the 9-pass LAGEOS data set. Fig. 12 displays a LAGEOS data set taken on October 20, 1981 with the microchannel PMT installed. Fig. 12(a) is a graph of the raw data set totaling 3707 range measurements of which 101 were rejected following ten iterations through the LASPREP processor. The single-shot rms of the edited data was 1.68 cm. Fig. 12(b) is a plot of the corresponding normal points which have an rms of only 0.3 cm. This is only slightly higher than what would be expected for a totally random error, i.e., $1.68 \text{ cm}/\sqrt{50} = 0.25$ cm. The peak-to-peak variation in the normal points was about $\pm$ 0.8 cm.

Satellite range tests have begun with the fully upgraded range receiver in Fig. 7. Preliminary results suggest a single-shot rms of 0.9 cm off the LAGEOS satellite [21] but the data is limited and has not yet been properly reduced

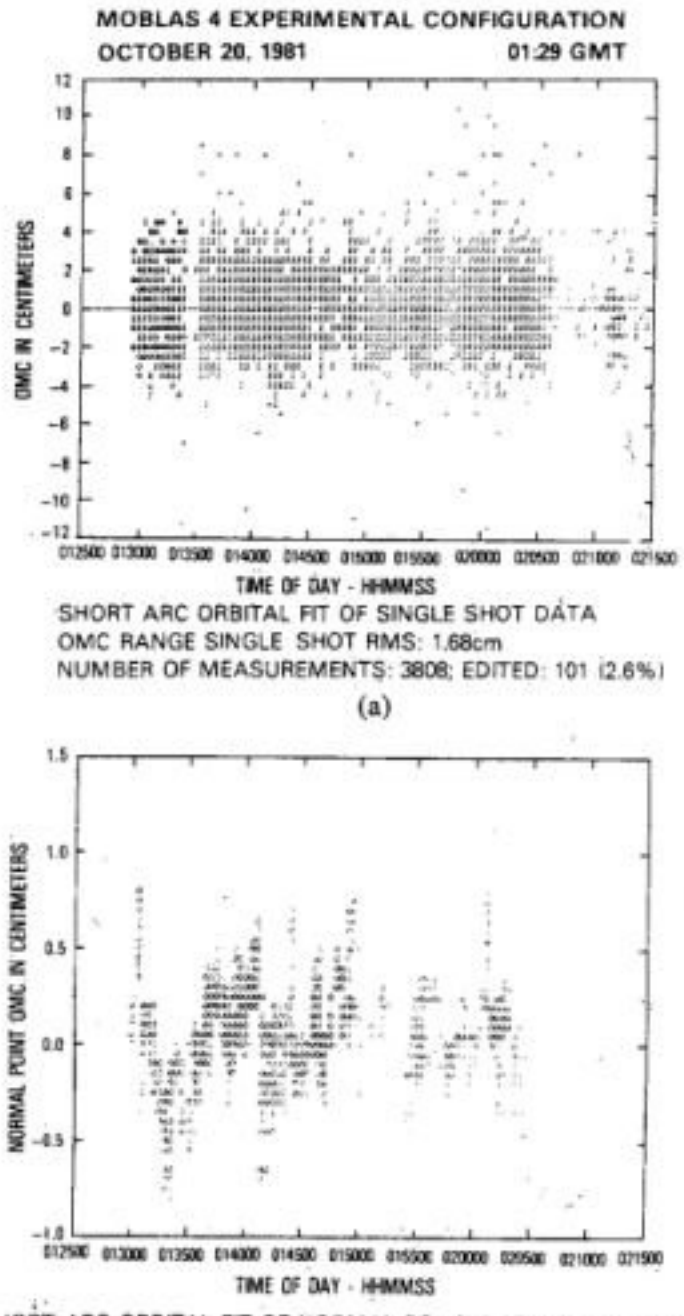

Fig. 12. Sample LAGEOS data with partially upgraded MOBLAS receiver (prototype Quantel 402DP mode-locked laser, prototype ITT 4129 MCP/PMT, ORTEC 934 CFD, HP5360 TIU).

and analyzed. Ground data over 1-km to a few-kilometer horizontal paths using the same or similar receivers have yielded unedited single-shot precisions between 5 and 10 mm. The long-term repeatability of the mean target range is on the order of a few millimeters.

V. Future Systems

A. Feasibility of Millimeter Accuracy Systems

Even if the ranging machine and the on-site calibration techniques were error free, efforts to convert time of flight to an absolute range accuracy at the millimeter level would be severely hampered by the uncertainties associated with the atmospheric channel. As pointed out in [16], however, dual-wavelength laser ranging systems, which utilize the dispersion in the atmospheric refractive index, can be used to directly measure the delay introduced by the atmosphere. In a two-color ranging system, the shorter wavelength (near ultraviolet) pulse is generated from the longer wavelength (visible or near infrared) in a nonlinear crystal. Thus they leave the ranging system simultaneously. As the pulses propagate through the atmosphere, a differential time delay is introduced by the atmospheric dispersion which is proportional to the integrated air density over the optical path. This differential delay will vary with atmospheric conditions, elevation angle, etc. For readily available lasers, the dispersive effect is about 10 percent of the delay at a single wavelength [16]. Thus to achieve 1-mm absolute range accuracy in the atmospheric channel, a timing accuracy of about 0.7 ps (700 fs) corresponding to an absolute range accuracy in a vacuum of 100 μm would be required. Since this represents a timing resolution about three orders of magnitude better than the impulse response of a microchannel-plate photomultiplier, the conventional PMT approach seems doomed to failure.

The only optical receivers which have subpicosecond time resolution are streak tubes. Linear streak tubes, with resolutions of 1 or 2 ps are commercially available and laboratory units having 0.25-ps timing resolution have been reported [22]. In a linear streak tube, the incoming pulse strikes a photocathode. The resulting photoelectrons are accelerated by a mesh electrode and deflected in one axis by a pair of plates which are subjected to a very fast voltage ramp. This results in a time-to-space mapping of the photoelectron distribution. The duration of the ramp or sweep defines the time window seen by the tube. The electrons are multiplied by a set of internal microchannel plates and accelerated onto a phosphor screen at the rear of the streak tube. The spatial distribution of the resulting image mirrors the temporal profile of the illuminating pulse. The operational characteristics of streak tubes and the results of some two-color differential delay measurements with a commercial 2-ps-resolution streak tube are discussed in a companion article by Abshire and Gardner [16].

The mode-locked Nd:YAG laser transmitters used in modern SLR systems are easily capable of generating 30-ps pulsewidths with sufficient output energy for satellite ranging but, because of the relatively slow 450-ps impulse response of the fastest high-gain photomultipliers, they are usually operated with much longer pulsewidths to reduce the risk of optical damage. The laser dyes and the solid-state vibronic-laser materials, such as Alexandrite, have sufficiently wide-gain bandwidths that subpicosecond pulsewidths are possible. In fact, laser pulses as narrow as 10 fs (1×10^{-14} s) have already been demonstrated in the laboratory using colliding pulse techniques in laser dyes—although certainly not with the peak powers necessary to range to satellites. Since one can usually time to a small fraction of the laser pulsewidth (< 10 percent), pulsewidths on the order of a few picoseconds should permit the subpicosecond timing required by millimeter-accuracy two-color ranging. Generation of the required energies (tens of millijoules) at these pulsewidths appears to be within the state of the art.

Thus the basic components required for millimeter-accuracy ranging exist. The problem then becomes one of integration. The approach being investigated at Goddard is the Optical Time Interval Unit.

B. Optical Time Interval Unit

The concept of the Optical Time Interval Unit (OTIU) is very similar to that of the electronic TIU described in Section II-D except that it uses optical rather than electronic pulses. It consists of a highly accurate optical clock,

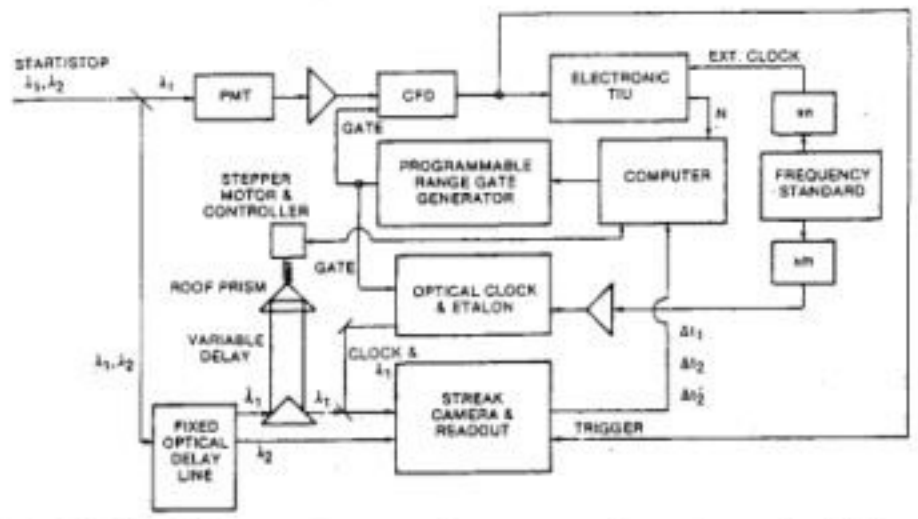

Fig. 13. Block diagram of a two-color range receiver using a single linear streak-camera interpolator.

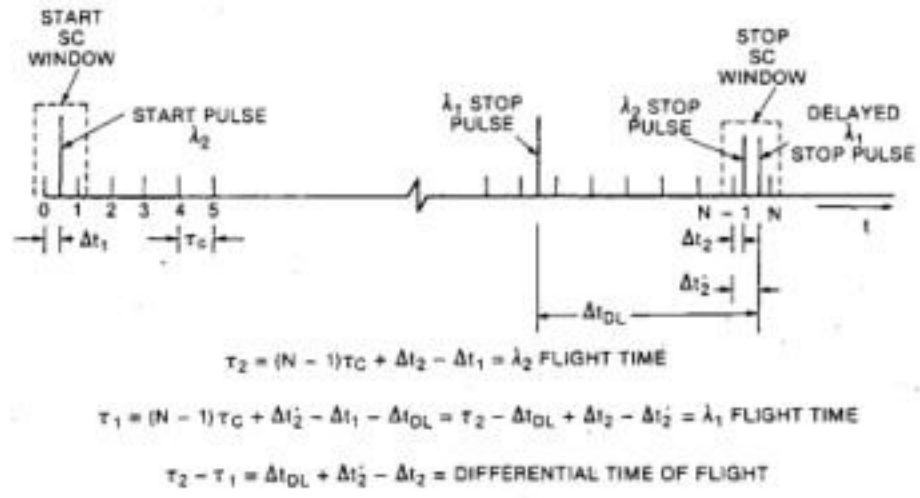

Fig. 14. Timing diagram for the two-color linear streak-camera receiver depicted in Fig. 13.

a pulse counter or scaler for obtaining the coarse time interval measurement T_{12}, and streak tube interpolators for measuring T_1 and T_2 with the required subpicosecond resolution. There are a number of possible geometries [23] but we will discuss the OTIU within the framework of a two-color ranging system which makes maximum utilization of existing ranging hardware and which allows for the operational needs of existing commercial streak cameras.

A range-receiver configuration which permits the two-color differential time delay to be measured with a single linear streak camera is described in Fig. 13. The corresponding timing diagram for the receiver is presented in Fig. 14. The two mode-locked pulses at wavelengths λ_1 and λ_2 leave the ranging instrument simultaneously, travel to the target through the atmosphere, and return separated in time by an amount $\tau_2 - \tau_1$. The signal strengths at the longer visible or near infrared wavelength λ_1 are usually greater so this is used to trigger the conventional single-color common-channel range receiver at the top of Fig. 13. The incoming start pulse is detected by a high-speed microchannel-plate photomultiplier (MCP/PMT), amplified, and input to a constant fraction discriminator (CFD). A gating voltage supplied by the system computer permits passage of the start pulse from the CFD to a conventional electronic TIU (e.g., the HP 5370A) which starts the "coarse" time interval measurement. Based on an *a priori* estimate of the expected range to the target, the computer supplies a second gating voltage to the CFD to permit passage of the "stop" logic pulse to the TIU. The output logic pulse of the CFD is also used to trigger the streak camera. Gating the CFD reduces the probability that background noise will trigger the receiver. The absolute timing accuracy of the HP5370A is on the order of 100 ps. The electronic TIU in Fig. 13 serves as the coarse scaler, or counter, for the OTIU and provides the integer $(N - 1)$ in Fig. 14 for the measured time interval. It is only necessary that the TIU be able to resolve the time of flight with a resolution better than the period of the optical clock to be described next.

An external master oscillator, accurate to a part in 10^{11} for LAGEOS distances, provides the clock pulses for the electronic TIU measurement. The master oscillator source is also multiplied electronically, amplified, and input to the "optical clock" which in turn generates a train of picosecond optical pulses which are then focused onto the slit of the streak camera. The master-clock output could be input to the terminal of a light-emitting diode (LED), a laser diode (LD) held just below threshold, or to the terminals of an acoustooptic or electrooptic modulator in an actively mode-locked laser transmitter. A picosecond-pulse laser diode is contemplated as the optical clock for the initial experiments at Goddard. The period of the optical clock must be shorter than the time window of the streak camera so that at least two clock images are captured during the sweep. The frequency of the optical train can be increased, if necessary, through the use of Fabry–Perot etalons. These can also be used to calibrate the linearity of the streak voltage ramp. To prevent saturation of the streak camera by the optical clock, the streak-camera gate pulse from the CFD can be used to trigger a Pockels cell gate to permit only a few optical clock pulses to enter the streak camera for a given range measurement.

The longer wavelength pulse λ_1 which is the first to return from the satellite, passes through a fixed optical delay line common to both wavelengths and then is reflected by a dichroic beamsplitter into a variable optical delay line. The fixed optical delay line compensates for a delay of about 30 ns between the trigger pulse and the actual voltage sweep in commercial streak cameras. It is possible, however, to trigger the streak camera by illuminating a silicon photoconductor with a fraction of the first optical clock pulse switched out of the train by the aforementioned Pockels cell. The silicon's electrical output pulse can be adjusted to give a voltage ramp with a delay of only 1–2 ps and a jitter under 1 ps [24]. The inconvenience caused by a trigger delay is avoided with two-axis circular-scan or single-axis "synchroscan" streak cameras which continuously view the incoming radiation. To date, circular-scan tubes have demonstrated only 6-ps resolution [25] and synchroscan tubes introduce additional ambiguities in the measurement.

The purpose of the variable optical delay line is to reduce the temporal separation of the two return pulses so that they both lie within the streak camera time window as in Fig. 14. The time delay Δt_{DL} of the variable delay line can be preset under automated control based on approximate *a priori* knowledge of target range and elevation angle. A satellite laser ranging system operating over elevation angles from 20°–90°, for example, would require variable delay paths from about 25–100 cm in length. One implementation of the delay line is a roof prism whose

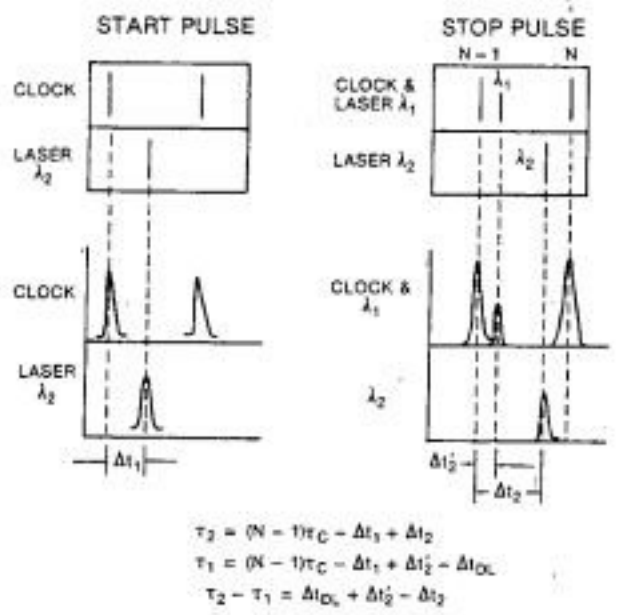

Fig. 15. Two-color streak-camera images showing spatially separated pulses.

position is controlled by means of a stepper motor-driven lead screw. The delay can be precisely set with few micrometers (femtoseconds) accuracy by counting the number of steps, computing the number of screw resolutions, and multiplying by the screw pitch. The variable delay can be adjusted on a shot to shot basis to keep the two returns within the streak camera window for all satellite ranges. An alternative to using predicted values for the atmospheric delay would be to utilize lower-resolution measurements from a multistop TIU or second electronic TIU to set the variable optical delay.

Since the start pulse at wavelength λ_1 also travels through the variable delay line, it is not recorded by the streak tube but, since it enters the receiver simultaneously with the pulse at wavelength λ_2, no information is lost. To avoid wavelength ambiguities, the two laser-pulse images are separated spatially in the optical delay line so that they illuminate separate points in the streak-camera slit. The optical clock pulses are superimposed (spatially) on the λ_1 image and are identifiable by their fixed temporal separation. This is readily done because commercial streak tubes permit separate readouts over two spatial regions of the slit. Furthermore, streak tubes are capable of processing the data from three or more spatial regions in the slit so that streak images of the two wavelengths can be totally isolated from the optical clock pulses and each other. Examples of the expected streak-camera images are illustrated in Fig. 15.

VI. Concluding Remarks

The present article has attempted to provide a tutorial review of the hardware currently in use or contemplated for use in operational satellite laser ranging systems. It appears highly likely that single-shot rms precisions of about 1 cm will soon be routinely achieved with single-color systems to well-designed ranging satellites such as LAGEOS, Starlette, and LAGEOS II, scheduled for launch by the Italians on a future shuttle mission. The key components required for millimeter-accuracy systems exist today, but much additional work is required to integrate them into an absolute-range-measurement machine and to evaluate their ability to correct for atmospheric biases which now appear to be a dominant error mechanism. It is hoped that a prototype two-color streak-camera-based range receiver will be available prior to the testing of LAGEOS II at Goddard in 1986 so that effects of the target geometry on such systems can be determined. Perhaps spherical target satellites having fewer but larger cube-corner reflectors would be better suited to achieving millimeter absolute accuracies. Such designs would further restrict the number of cubes contributing to the return while retaining a high radar cross section.

Potential future developments that have not been reviewed in the present article include the use of laser ranging instruments from airborne [26], [27] or spaceborne platforms [28]. These are potentially cost effective approaches to gathering large amounts of geophysical data through the replacement of expensive ground systems with relatively inexpensive passive retroreflectors.

Acknowledgment

The material presented in this article has been amassed through years of close interaction with a highly talented group of colleagues at the NASA Goddard Space Flight Center in Greenbelt, MD, and much of their work is referenced here. In strictly alphabetical order, they are Dr. J. B. Abshire, Dr. M. W. Fitzmaurice, T. S. Johnson, J. Friskey McGarry, P. O. Minott, D. A. Premo, H. E. Rowe, Dr. D. Smith, and T. W. Zagwodzki. The author has also benefitted from many discussions with his former thesis advisor, Dr. C. Alley of the University of Maryland, especially in the areas of lunar laser ranging systems and applications.

References

[1] H. H. Plotkin, T. S. Johnson, P. L Spadin, and J. Moye, "Reflection of ruby laser radiation from explorer XXII" *Proc. IEEE*, vol. 53, pp. 301–302, Mar. 1965.

[2] "The NASA geodynamics program: An overview," Geodynamics Program Office, NASA Headquarters, Washington, DC, NASA Tech. Paper 2147, Jan. 1983.

[3] J. D. Mulholland, "Scientific achievements from ten years of lunar laser ranging," *Rev. Geophys. Space Phys.*, vol. 18, pp. 549–564, Aug. 1980.

[4] C. O. Alley, "Laser ranging to retro-reflectors on the moon as a test of theories of gravity," in *Quantum Optics, Experimental Gravity, and Measurement Theory*, P. Meystre and M. O. Scully, Eds New York: Plenum, 1983, pp. 429–495.

[5] E. C. Silverberg, "Operation and performance of lunar laser ranging station," *Appl. Opt.*, vol. 13, pp. 565–573, Mar. 1974.

[6] M. E. Shawe and A. G. Adelman, "Precision laser tracking for global and polar motion," *IEEE Trans. Geosci. Remote Sensing*, this issue, pp. 391–397.

[7] E. C. Silverberg and D. L. Byrd, "A mobile telescope for measuring continental drift," *Sky Telesc.*, vol. 61, pp. 405–408, May 1981.

[8] J. J. Degnan and T. W. Zagwodzki, "Characterization of the *Q*-switched MOBLAS laser transmitter and its ranging performance relative to a PTM *Q*-switched system," NASA Goddard Space Flight Center, Greenbelt, MD, NASA Tech. Memo. 80336, Oct. 1979.

[9] —— "A comparative study of several transmitter types for precise laser ranging," in *Proc. 4th Int. Workshop Laser Ranging Instrument*. (University of Texas, Austin, Oct. 12–16, 1981). Bonn: Geodetic Institute, University of Bonn, 1982, pp. 241–250.

[10] J. B. Abshire, NASA Goddard Space Flight Center, Greenbelt, MD, unpublished.

[11] J. J. Degnan, T. W. Zagwodzki, and H. E. Rowe, "Satellite laser

ranging experiments with an upgraded MOBLAS station," in *Proc. 5th Int. Workshop Laser Ranging Instrument*. (Royal Greenwich Observatory, East Sussex, England, Sept. 10–14, 1984), to be published.
[12] T. W. Zagwodzki, NASA Goddard Space Flight Center, Greenbelt, MD, unpublished.
[13] B. T. Turko, "Multichannel interval timer," Lawrence Berkeley Laboratories, Berkeley, CA, unpublished.
[14] B. Turko, "A picosecond resolution time digitizer for laser ranging," *IEEE Trans. Nucl. Sci.*, vol. NS-25, pp. 75–80, Feb. 1978.
[15] M. W. Fitzmaurice, P. O. Minott, J. B. Abshire, and H. E. Rowe, "Prelaunch testing of the laser geodynamic satellite (LAGEOS)," NASA Goddard Space Flight Center, Greenbelt, MD, NASA Tech. Paper 1062, Oct. 1977.
[16] J. B. Abshire and C. S. Gardner, "Atmospheric refractivity corrections in satellite laser ranging," *IEEE Trans. Geosci. Remote Sensing*, this issue, pp. 414–425.
[17] J. B. Abshire, "Pulsed multiwavelength laser ranging system," NASA Goddard Space Flight Center, Greenbelt, MD, NASA Tech. Memo. 83917, Mar. 1982.
[18] E. C. Silverberg, "The feedback calibration of the TLRS ranging system," in *Proc. 4th Int. Workshop Laser Ranging Instrument*. (University of Texas, Austin, Oct. 12–16, 1981). Bonn: Geodetic Institute, University of Bonn, 1982, pp. 331–337.
[19] T. W. Zagwodzki, J. F. McGarry, J. J. Degnan, R. S. Chabot, J. G. Lessner, and J. B. Abshire, "An experimental large aperture satellite laser ranging station at GSFC," in *Proc. 5th Int. Workshop Laser Ranging Instrument*. (Royal Greenwich Observatory, East Sussex, England, Sept. 10–14, 1984), to be published.
[20] O. J. Oaks, J. A. Buisson, and S. C. Wardrip, "GPS time transfer receivers for the NASA transportable laser ranging network," in *Proc. 4th Int. Workshop Laser Ranging Instrument*. (University of Texas, Austin, Oct. 12–16, 1981). Bonn: Geodetic Institute, University of Bonn, 1982, pp. 338–351.
[21] T. Varghese, Bendix Field Engineering Corporation, Greenbelt, MD, private communication.
[22] W. Sibbett, H. Niu, and M. R. Baggs, "Femtosecond streak image tube," in *Proc. 15th Int. Congress High Speed Photog. Photon*. (San Diego, CA, Aug. 21–27, 1982), pp. 271–275.
[23] J. B. Abshire and J. J. Degnan, Patent disclosure, Nov. 2, 1983, unpublished.
[24] W. Knox, G. Mourou, and S. Letzring, "Jitter-free signal averaging streak camera," in *Proc. 15th Int. Congress High Speed Photog. Photon*. (San Diego, CA, Aug. 21–27, 1982), pp. 308–312.
[25] W. E. Sleat, "Photochron 2C streak-camera for spaceborne laser ranging," in *Proc. 5th Int. Workshop Laser Ranging Instrument*. (Royal Greenwich Observatory, East Sussex, England, Sept. 10–14, 1984), to be published.
[26] J. J. Degnan, W. D. Kahn, and T. S. Englar, Jr., "Centimeter precision airborne laser ranging system," *J. Survey. Engineer.* vol. 109, no. 2, pp. 99–115, Aug. 1983.
[27] W. D. Kahn, J. J. Degnan, and T. S. Englar, Jr., "The airborne laser ranging system, its capabilities and applications," *Bull. Geodet.* vol. 57, pp. 180–194, 1983.
[28] J. J. Degnan, "An overview of NASA airborne and spaceborne laser ranging development," in *Proc. 5th Int. Workshop Laser Ranging Instrument*. (Royal Greenwich Observatory, East Sussex, England, Sept. 10–14, 1984), to be published.

John J. Degnan, III, received the B.S. degree in physics from Drexel University in 1968 and the M.S. and Ph.D. degrees in physics from the University of Maryland in 1970 and 1979, respectively. His doctoral dissertation was on the analysis, numerical simulation, and development of high-peak-power ultrashort-pulse solid-state laser systems for ranging applications.

He is presently Head of the Advanced Electrooptical Instrument Section (Code 723.2) at NASA's Goddard Space Flight Center, Greenbelt, MD, where he has been employed since 1964 when, as a cooperative student from Drexel University, he participated in the first laser ranging experiments to the Beacon Explorer B satellite. He is the author of over 40 journal articles or technical reports on lasers, laser applications, optical heterodyne detection, spectroscopy, and nonlinear optics and is included in several lists of leading technologists.

Dr. Degnan is a member of the American Physical Society, the Optical Society of America, and Sigma Pi Sigma and serves on the Editorial Review Board of the IEEE TRANSACTIONS ON INSTRUMENTATION AND MEASUREMENT.